Physica A 527 (2019) 121326

Contents lists available at ScienceDirect

Physica A

journal homepage: www.elsevier.com/locate/physa

Finite-field phase transitions and criticality in a generalized kagomé Ising ferromagnet: Exact solutions

J.H. Barry, K.A. Muttalib *

Department of Physics, University of Florida, Gainesville, FL 32611-8440, United States

HIGHLIGHTS

- Exact solutions of a 3-parameter model of a kagomé Ising ferromagnet.
- Model includes pair and triplet interactions and a magnetic field.
- Exact ground state and thermal phase diagrams obtained.
- Field induced transition can identify existence/importance of triplet interactions.
- Generalized fluid–magnet relations allow exact solutions of associated fluid model.

ARTICLE INFO

Article history:
Received 9 June 2018
Received in revised form 25 April 2019
Available online 29 April 2019

Keywords:
Ising model
Triplet interactions
Exact phase diagrams
Ferromagnetism

ABSTRACT

The standard two-parameter (nearest-neighbor pair-interaction J_2 and magnetic field h) planar Ising model ferromagnet only has phase transitions in zero field. We generalize a standard kagomé Ising model ferromagnet by adding localized triplet Ising interactions J_3. Exact solutions are obtained for the phase diagrams of the three-parameter model, demonstrating finite-field phase transitions and criticality. Necessary conditions for the latter findings include the pair-interaction parameter being ferromagnetic ($J_2 > 0$), the applied field parameter competing against the intrinsic triplet-interaction parameter, the ratio of the triplet- and pair-interaction parameters residing within a determined finite symmetrical interval, and the field parameter being properly tuned, viz., tracing the pertinent field vs temperature phase boundary curve. The curvilinear shape of the phase boundary facilitates the relative strength $|J_3|/J_2$ of the triplet interaction to be experimentally accessible. Employing generalized fluid–magnet correspondence relations, it is mathematically convenient and informative to affiliate the above magnetic phase diagrams with the corresponding fluid phase diagrams of the associated generalized kagomé lattice-gas model.

1. Introduction

In statistical theories of highly cooperative systems, say, in phase transitions and critical phenomena, the standard two-parameter (nearest-neighbor pair interaction and magnetic field) planar Ising model is distinctive [1]. In zero magnetic field, it still prevails as the most realistic lattice-statistical model of phase transitions and criticality for which exact solutions can be obtained for both thermodynamic quantities and correlations [2]. However, while various numerical techniques have been developed [3–7], no exact solution for the planar Ising model has been found in the presence of a finite magnetic field, despite many decades of efforts.

* Corresponding author.
E-mail addresses: barry@phys.ufl.edu (J.H. Barry), muttalib@phys.ufl.edu (K.A. Muttalib).

https://doi.org/10.1016/j.physa.2019.121326
0378-4371/

The standard planar Ising model can be generalized to contain higher-order Ising interactions. Indeed, any Hamiltonian having a finite density of finitely discrete commuting local variables can be cast as an Ising model. A simple physical extension would be the addition of localized *triplet Ising interactions* [8–14]. Triplet interactions are pervasive in nature [15–18], can be either attractive or repulsive, and not always negligible in strength compared to pair interactions especially in the modern era of fabricated materials and cold-atom technology with optical lattices [19–21], the above being active and ongoing research fields with widespread applications. More importantly, though, it develops that adding triplet interactions to the standard two-parameter kagomé Ising model ferromagnet allows one to obtain *exact phase diagrams* at finite fields. Although the field in this case is not an independent variable in the solution and has to be tuned, exact solutions of such a generalized Ising model provides important insights into certain types of 'finite-field induced phase transitions'. Such effects may lead to increased experimental efforts in finding or fabricating novel materials with non-negligible triplet interactions.

In the current paper, one theoretically investigates the magnetic canonical partition function of a generalized kagomé Ising model. The generalized Ising model has not only magnetic field and nearest-neighbor pair interactions but also triplet "interaction round-a-face" (IRF) [22] for each elementary triangle of the kagomé lattice. The method employed is premised upon exact results obtained by Wu [23], Wu and Wu [24] and Lin and Chen [25]. The authors established that the partition function of the current generalized (three-parameter) kagomé Ising model is equivalent, aside from known prefactors, to the partition function of a standard (two-parameter) honeycomb Ising model with pair interactions and field. Utilizing a weak-graph transformation, their theoretical developments [26,27] incorporated a honeycomb symmetric eight-vertex model in a mediating role [28]. The grand partition function of a kagomé lattice-gas model with pair and triplet interactions [29] (*generalized kagomé lattice-gas model*) is equivalent to the partition function of an associated eight-vertex model which itself can be transformed, aside from known prefactors, into a partition function of a standard honeycomb Ising model. (One remarks, neglecting triplet interactions, it is well-known that the half-filled lattice-gas identifies with the Ising magnet in zero field). Towards the goal of determining phase diagrams of the generalized kagomé Ising ferromagnet, a theory is formulated which first obtains similar exact phase diagrams of the generalized kagomé lattice-gas model, and then employs generalized fluid–magnet simple correspondence relations to attain the goal ("deux d'un coup").

For both generalized models (magnet/fluid) on the kagomé lattice, the present investigations determine all possible continuous and discontinuous phase transitions (*exact phase diagrams*). Due to the presence of triplet interactions, the resulting temperature plots of phase boundaries and diameters of coexistence regions exhibit curvilinear portraits contrasting the corresponding familiar rectilinear (i.e., straight) portraits of the standard models. In the corresponding generalized kagomé Ising model with ferromagnetic pair interactions, this implies that *finite-field phase transitions and criticality* can occur provided that the applied magnetic field parameter competes with the intrinsic triplet-interaction parameter, and the field is properly tuned, viz., tracing the pertinent field vs temperature phase boundary curve. The curvilinear form of the field-temperature phase boundary determines a range of field values within which, for a fixed magnetic field, one crosses the phase boundary at a fixed temperature that depends on the ratio of the strengths of the triplet and pair interactions. Systematically exploring the phase boundary experimentally would therefore provide a direct way to not only just detect, but also to determine the relative magnitude of triplet interaction even in the presence of a dominant pair-interaction in a given magnetic system.

To encounter phase transitions and criticality, the ratio values of the three- and two-spin interaction parameters necessarily reside within a determined finite symmetrical interval. For antiferromagnetic pair interactions, no phase transitions exist. To our knowledge, although there are a few interesting exactly solved models either with a pair interaction and a magnetic field [30] or with a triplet interaction and a magnetic field [31], the literature in statistical physics and magnetism lacks any other examples for planar lattice models of magnets with field, pair- and triplet-interactions (or corresponding generalized fluid models) whose phase diagrams are known exactly.

The balance of the paper is organized as follows. Section 2 introduces the generalized Ising model on a kagomé lattice and Section 3 provides the background and known results on which the current work is based. Section 4 establishes generalized fluid–magnet correspondences. In Section 5, the ground state phase diagrams are obtained for the generalized lattice-gas model and the generalized Ising magnet. Section 6 affords a comparatively transparent implementation of the theory, obtaining exact phase diagrams for a special case of competing interactions. Section 7 considers the general case of arbitrary values of competing interactions. Section 8 is a short discussion and summary. A direct proof of the equivalence of the partition function of the honeycomb eight-vertex model with the current grand partition function of the generalized kagomé lattice-gas model is included in Appendix A, while details of the calculations of the ground state phase diagrams and the coexistence curves are shown in Appendices B and C, respectively.

2. The generalized Ising model

Consider a kagomé lattice (Fig. 1, solid edges) of $\mathcal{N}$ sites, and an Ising model Hamiltonian H_I given by

$$-H_I = h\sum_i \sigma_i + J_2 \sum_{\langle i,j\rangle} \sigma_i\sigma_j + J_3 \sum_{\langle i,j,k\rangle} \sigma_i\sigma_j\sigma_k \tag{1}$$

where $\sigma_l = \pm 1, \quad l = 0, 1, \ldots, \mathcal{N}-1$ are the Ising variables, the summation $\sum_{\langle i,j\rangle}$ is taken over all distinct nearest-neighbor pairs of sites of a kagomé lattice and $\sum_{\langle i,j,k\rangle}$ over all triplets of sites belonging to elementary triangles. The

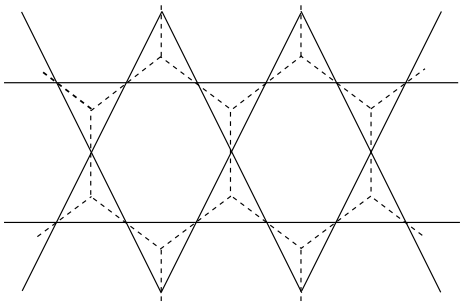

Fig. 1. A kagomé lattice (solid edges) is a two-dimensional periodic array of equilateral triangles and regular hexagons. The lattice is semiregular [33] (all vertices equivalent, all edges equivalent, but not all faces equivalent) and has coordination number 4. A honeycomb lattice (dashed edges) can be associated with the kagomé lattice. The mid-points of the edges of the honeycomb lattice may be viewed as the vertices of the kagomé lattice. The kagomé lattice is thus termed the *covering lattice* of the honeycomb lattice.

magnetic field parameter [32] is h, and the pair interaction $J_2 > 0$ represents a ferromagnetic interaction such that in the absence of both h and the triplet interaction J_3, the model is exactly soluble with an ordered phase at zero temperature and a ferromagnetic–paramagnetic phase transition at a finite critical temperature [2]. Without the triplet interaction, the Ising model with pair interactions in a field has not been solved exactly, despite many decades of efforts. It is somewhat counter-intuitive that including the triplet interaction in addition to the magnetic field allows exact solutions of phase diagrams in this highly correlated model. Although for fixed values of J_2 and J_3, the values of h are not independent but must be tuned, nevertheless the exact solutions provide important insights into the long-standing problem of finite-field phase transitions.

The canonical partition function of (1) is

$$\begin{aligned} &Z(L,K,M) \equiv Tr_\sigma\, e^{-\beta H_I} \\ &= e^{L\sum_i \sigma_i + K\sum_{\langle i,j\rangle}\sigma_i\sigma_j + M\sum_{\langle i,j,k\rangle}\sigma_i\sigma_j\sigma_k} \end{aligned} \tag{2}$$

where $\beta \equiv 1/k_BT$ is the 'inverse temperature' and

$$L \equiv \beta h, \quad K \equiv \beta J_2, \quad M \equiv \beta J_3. \tag{3}$$

As will be shown below, the mathematical technique employed here involves a mapping of $Z(L,K,M)$ to the partition function of an Ising model on the associated honeycomb lattice *without triplet interactions*, via the grand canonical partition function of a generalized kagomé lattice-gas model. This, as a bonus, allows for the evaluation of exact phase diagrams for the condensation of a kagomé lattice-gas with two- and three-particle interactions. An intrinsic symmetry of the partition function

$$Z(L,K,M) = Z(-L,K,-M) \tag{4}$$

can easily be proven by global inversion $\sigma_l \to -\sigma_l$ of the Ising summation (dummy) variables in the definition (2). This symmetry will be useful later in the study of the zero temperature phase diagram.

In the next section we briefly outline the mapping.

3. Equivalences of partition functions

The partition function of the three-parameter Ising model (1) on a kagomé lattice (Fig. 1, solid edges) can be mapped, by means of a honeycomb eight-vertex model partition function, to the partition function of a standard two-parameter Ising model on the associated honeycomb lattice (Fig. 1, dashed edges) with exactly renormalized pair-interaction and field. The latter can be aptly solved for phase transitions and criticality under the necessary zero-field condition. While this mapping can be done directly, it is easier, and in fact more useful for the present purposes, to employ an already known mapping via a generalized lattice-gas model, as described below.

3.1. Generalized kagomé lattice-gas model

Consider a kagomé lattice (Fig. 1, solid edges) of $\mathcal{N}$ sites, embedding a lattice gas having both two- and three-particle interactions. The model Hamiltonian H_{lg} is given by

$$-H_{lg} = \epsilon_2 \sum_{\langle i,j\rangle} n_i n_j + \epsilon_3 \sum_{\langle i,j,k\rangle} n_i n_j n_k, \tag{5}$$

where ϵ_2, ϵ_3 are pair and triplet interaction parameters, respectively. The summation $\sum_{\langle i,j\rangle}$ is taken over all distinct nearest-neighbor pairs of sites, and $\sum_{\langle i,j,k\rangle}$ over all triplets of sites belonging to elementary triangles. The lattice gas variables n_l are idempotent site-occupation numbers defined as $n_l = 1$ if site l is occupied and 0 if site l is empty. In (5), an infinitely strong (hard-core) repulsive pair potential has also been tacitly assumed for atoms on the *same* site, thereby preventing multiple occupancy of any site as reflected in the dichotomic values of the occupation numbers.

In the usual context of the grand canonical ensemble, one introduces

$$\mathcal{H} = H_{lg} - \mu N, \tag{6}$$

where μ is the chemical potential with N being the conjugate total number of particles

$$N = \sum_i n_i, \quad i = 0, 1, \ldots, \mathcal{N} - 1. \tag{7}$$

One therefore obtains the grand canonical partition function $\Xi(\mu, \mathcal{N}, T)$ as

$$\Xi(\mu, \mathcal{N}, T) \equiv Tr_n e^{-\beta\mathcal{H}} = Tr_n e^{\beta\mu\sum_i n_i} \times e^{K_2\sum_{\langle i,j\rangle} n_i n_j + K_3\sum_{\langle i,j,k\rangle} n_i n_j n_k} \tag{8}$$

where

$$K_2 \equiv \beta\epsilon_2; \quad K_3 \equiv \beta\epsilon_3. \tag{9}$$

For later use, it will be useful to represent the parameters of the generalized lattice-gas model as

$$x \equiv e^{K_2}; \quad y \equiv e^{K_3}; \quad z \equiv e^{\beta\mu} \quad \text{(fugacity)}. \tag{10}$$

By changing from the Ising variable representation σ_l in (1) to an occupation-number representation n_l of the lattice-gas via the local transformations

$$n_l = \frac{1}{2}(1 + \sigma_l), \quad \sigma_l = \pm 1, \quad l = 0, 1, \ldots, \mathcal{N} - 1, \tag{11}$$

it was shown in [29] that the grand canonical partition function $\Xi(\mu, \mathcal{N}, T)$ in (8) can be related to the magnetic canonical partition function $Z(L, K, M)$ as

$$\Xi(\mu, \mathcal{N}, T) = e^{(L-2K+2M/3)\mathcal{N}} Z(L, K, M) \tag{12}$$

where $Z(L, K, M)$ is the magnetic canonical partition function given in (2), with

$$L = K_2 + \frac{K_3}{4} + \frac{\beta\mu}{2}, \quad K = \frac{K_2}{4} + \frac{K_3}{8}, \quad M = \frac{K_3}{8}. \tag{13}$$

3.2. Equivalence of $\Xi(\mu, \mathcal{N}, T)$ and $Z_{8V}(a, b, c, d)$

Ref. [29] showed that $\Xi(\mu, \mathcal{N}, T)$ is equivalent to the partition function of a honeycomb eight-vertex model $Z_{8V}(a, b, c, d)$,

$$\Xi(\mu, \mathcal{N}, T) = Z_{8V}(a, b, c, d) \tag{14}$$

where

$$a = x^3 y z^{3/2}; \quad b = xz; \quad c = \sqrt{z}; \quad d = 1 \tag{15}$$

and x, y and z are defined in (10).

While relation (14) was earlier established in [29], a more direct proof has now been obtained by us which we include in Appendix A.

3.3. Equivalence of $Z_{8V}(a, b, c, d)$ and $Z^*(L^*, K^*)$

Consider a standard Ising model defined on the associated honeycomb lattice (Fig. 1, dashed edges) of $\mathcal{N}^*(= 2\mathcal{N}/3)$ sites, with a Hamiltonian H^*_{hc} given by

$$-\beta H^*_{hc} = L^* \sum_i \mu_i + K^* \sum_{\langle ij\rangle} \mu_i \mu_j, \tag{16}$$

where each site-localized Ising variable $\mu_l = \pm 1$, $l = 1, \ldots, \mathcal{N}^*$, and L^*, K^* are (dimensionless) parameters for the magnetic field and nearest-neighbor pair interaction, respectively. The magnetic canonical partition function of the model

(16) is then given by

$$Z^*(L^*, K^*) = Tr_\mu e^{-\beta H^*_{hc}} = Tr_\mu e^{L^* \sum_i \mu_i + K^* \sum_{\langle i,j \rangle} \mu_i \mu_j} \tag{17}$$

where the trace symbol μ represents the set of total $\mathcal{N}^*$ Ising variables (no confusion with the chemical potential in (6) should arise). It is known [23,24,34] that the magnetic partition function (17) is related to the honeycomb eight-vertex model $Z_{8V}(a, b, c, d)$ as

$$Z_{8V}(a, b, c, d) = (a^*/2\cosh L^*)^{\mathcal{N}^*} (\cosh K^*)^{-3\mathcal{N}^*/2} \times Z^*(L^*, K^*). \tag{18}$$

where

$$\tanh L^* = \frac{V}{U}\left(\frac{\delta - A + C}{\delta + A - C}\right)^{1/2}, \tag{19a}$$

$$e^{2K^*} = \frac{\delta}{|C - A|}, \tag{19b}$$

$$a^* = \frac{FU}{B(1+\eta^2)^{3/2}}, \tag{19c}$$

with

$$A = c^2 - bd, \quad B = ad - bc, \quad C = ac - b^2, \tag{20a}$$

$$\eta = -\frac{A + C}{B} + \frac{\delta}{B} sgn(C - A), \tag{20b}$$

$$\delta = [(A + C)^2 + B^2]^{\frac{1}{2}}; \quad F = \eta(B\eta + 2C), \tag{20c}$$

$$U = (b + d)\eta + a + c, \tag{20d}$$

$$V = (a + c)\eta - (b + d) \tag{20e}$$

and vertex weights a, b, c, d are given by (15) and (10). In terms of the parameters x, y, z defined in (10), the pair-interaction parameter K^* is given by [29]

$$4K^* = \ln\left[1 + \frac{x^2 z l}{[x^2 z(xy - 1) + x - 1]^2}\right], \tag{21}$$

where

$$l \equiv l(x, y) = (x^2 y - 1)^2 - 4(x - 1)(xy - 1). \tag{22}$$

Note that ferromagnetic $K^* > 0$ requires that $l > 0$ in (21).

3.4. Central equivalence of $\Xi(\mu, \mathcal{N}, T)$ and $Z^*(L^*, K^*)$, and zero field condition $L^* = 0$

Combining (14) and (18), we finally obtain, aside from known prefactors, the central equivalence relation

$$\Xi(\mu, \mathcal{N}, T) = \left(\frac{a^*}{2\cosh L^*}\right)^{\mathcal{N}^*} \left(\frac{1}{\cosh K^*}\right)^{\frac{3\mathcal{N}^*}{2}} \times Z^*(L^*, K^*). \tag{23}$$

between the partition function of a generalized kagomé lattice-gas model and the partition function of a standard honeycomb Ising model in a magnetic field, the latter Ising model extensively studied in the literature and whose known exact solutions have essential importance throughout the present investigations. In the case of ferromagnetic interactions ($K^* > 0$) in (16), the *zero-field condition* $L^* = 0$ is a necessary condition for the existence of a phase transition (if $L^* \neq 0$, it is well known [35], in the thermodynamic limit, that there is no finite temperature singular behavior in the ferromagnetic Ising model free energy per spin, f, where $-\beta f = \lim_{N\to\infty} \frac{1}{N} \ln Z^*(L^*, K^*)$).

From (19a), the zero-field condition $L^* = 0$ in $Z^*(L^*, K^*)$ is equivalent to the $V = 0$ condition, V given by (20e). As shown in Ref. [29], this in turn is equivalent to the following cubic algebraic equation in the fugacity z:

$$z^3 + a_2 z^2 + a_1 z + a_0 = 0, \tag{24a}$$

with *real* coefficients

$$a_2 = \frac{3(x^2 y - 2xy + 1)}{x^3 y(x^3 y^2 - 3xy + 2)}, \tag{24b}$$

$$a_1 = -\frac{3(x^2y - 2x + 1)}{x^5y(x^3y^2 - 3xy + 2)}, \tag{24c}$$

$$a_0 = -\frac{(x^3y - 3x + 2)}{x^6y(x^3y^2 - 3xy + 2)}, \tag{24d}$$

where x, y and z defined in (10) are the parameters of the generalized lattice-gas model. Indeed, existence of this cubic equation as a condition for phase transitions makes it easier to study the overall phase transition problem in either of the magnetic models by first considering the associated phase diagrams for lattice-gas condensation described by $\Xi(\mu, \mathcal{N}, T)$. In the following Section, generalized fluid–magnet correspondence relations will be obtained which will allow the lattice-gas results to be interpreted in terms of the Ising magnet model (1) and vice versa.

4. Generalized fluid-magnet correspondences

The relations (13) between the parameters of the generalized magnet (1) and the generalized fluid (5) effectuate a generalized fluid–magnet correspondence. The one-to-one mapping between fluid and magnetic phase boundaries is direct and valuable. More definitely, let

$$\epsilon_3 \equiv -\alpha\epsilon_2, \quad J_3 \equiv -\alpha' J_2 \tag{25}$$

define the parameters α and α'. Using (9) and (10), this implies

$$y = x^{-\alpha}. \tag{26}$$

In addition, (3), (9), (13) and (25) can be combined using algebraic manipulations to yield the fluid–magnet correspondence

$$\frac{h}{J_2} = \frac{4}{2-\alpha}\left(\frac{\mu}{\epsilon_2} + \frac{4-\alpha}{2}\right). \tag{27}$$

The relation between α and α' turns out to be simply given by

$$\alpha' = \frac{\alpha}{2-\alpha}. \tag{28}$$

It is useful to define the *reduced temperature* t for the generalized kagomé lattice-gas model as

$$t \equiv \frac{K_{2c}^0}{K_2}, \tag{29}$$

where $K_2 = \beta\epsilon_2$ (9) and K_{2c}^0 is a known critical constant [36] for $\alpha = 0$ ($\epsilon_3 = 0$), viz., $K_{2c}^0 = \ln(3 + 2\sqrt{3}) = 1.86626\cdots$. In (29) one assumes that $\epsilon_2 > 0$ (the case $\epsilon_2 < 0$ is considered later). Similarly, the reduced temperature t' for the generalized Ising model is defined as

$$t' \equiv \frac{K_c^0}{K}, \tag{30}$$

where $K = \beta J_2$ (3) and K_c^0 is a known critical constant [36] for $\alpha' = 0$ ($J_3 = 0$), viz, $K_c^0 = \frac{1}{4}\ln(3 + 2\sqrt{3}) = 0.46656\cdots$. Note that $J_2 > 0$ for *all* cases of magnetic phase transitions and criticality (see Fig. 2(b)).

Relating t to t', one obtains a simple correspondence,

$$t' = \frac{2}{2-\alpha}t, \quad \epsilon_2 > 0. \tag{31}$$

As indicated earlier, for completeness, the cases $\epsilon_2 < 0$ need to be examined separately in relating t and t'. Consider the 2nd quadrant of ϵ_2–ϵ_3 space, particularly the dominant attractive wedge $3 < \alpha < \infty$ (see Fig. 2(a)). Since $\epsilon_2 < 0$, the *reduced temperature* t is defined as $t \equiv \frac{K_{2c}^0}{|K_2|}$. Then, as before, one obtains

$$t' = \frac{2}{\alpha-2}t, \quad \epsilon_2 < 0. \tag{32}$$

The "shift and rescale" correspondence relation (27) directly associates a *magnetic phase boundary* (reduced magnetic field h/J_2 vs reduced temperature t') with a *liquid–vapor phase boundary* (reduced chemical potential μ/ϵ_2 vs reduced temperature t) for a select value of α (or α'). The local change of variables in (11) initiated the derivation of the α, α' transformations (28). The derivation did not employ partial traces or "thinning" of the number of degrees of freedom in the models. The approach thus contrasts, say, familiar renormalization-group methods for locating and investigating criticality. Notwithstanding, the simple non-linear algebraic transformation (28) possesses two *fixed-points* $\alpha = \alpha' = 0,\ 1$.

The fluid–magnet mapping (27) between phase-boundaries is now extended to include the mapping between coexistence curves. A detailed derivation for a *liquid–vapor coexistence curve* (particle number density ρ vs reduced temperature

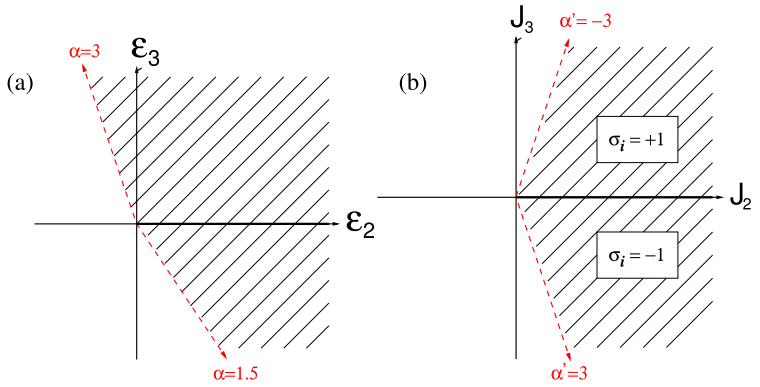

Fig. 2. Ground state phase diagrams for the generalized (a) fluid and (b) magnet. The regions of long-range order are shaded by oblique lines, while the vacant regions are disordered (devoid of long-range order). The parameter α in (a) is defined by the ray-line form $\epsilon_3 = -\alpha\epsilon_2$, and parameter α' in (b) is defined by the ray-line form $J_3 = -\alpha' J_2$. The dashed (red) lines, $\alpha = 3$ and $\alpha = 1.5$ in (a) and $\alpha' = \pm 3$ in (b), are discontinuous (first-order) transition lines as is the solid (black) line $\alpha = 0$. However, the dashed lines do not extend into finite temperatures whereas the solid line extends as a first-order surface (due to a non-vanishing surface tension).

t) will be developed in Section 6 for a specific value of α. Presently, the mapping or one-to-one correspondence with a *magnetic coexistence curve* (magnetization m vs reduced temperature t') for relevant values of α' can be found forthwith via thermal averaging of the local transformation (11). Specifically,

$$m = 2\rho - 1, \tag{33}$$

where the dimensionless magnetization is defined as $m \equiv \langle \sigma_l \rangle$ and the particle number density is defined as $\rho \equiv \langle n_l \rangle$.

Now that the generalized fluid–magnet correspondences have been established, it is more convenient to first consider the thermal phase diagrams of the two-parameter lattice-gas model (5) and then use (27), (28), (31) and (32) to obtain the magnetic phase diagrams of (1). This procedure will be used in the following sections.

5. Ground state phase diagrams

Given the fluid–magnet correspondences, we start with the two-parameter lattice gas model (5). However, before considering the thermal phase diagrams of (5), it is important to locate the ordered regions in its ϵ_2–ϵ_3 interaction parameter space that underlie or support thermal phase transitions and criticality. Other regions in ϵ_2–ϵ_3 space are disordered, i.e., devoid of long-range order. More markedly, we systematically establish the ground state (zero temperature) phase diagram. In these pursuits, the approach will be to take the zero temperature limit ($T \to 0$) of relevant finite-temperature expressions, with the convenient parametrization of the interaction parameters given in (25).

Assuming the zero-field condition $L^* = 0$ with its consequent cubic equation for the fugacity, one examines the zero-temperature limits of K^* and compares them with the known literature critical value [36] $K_c^* = \frac{1}{2}\ln(2+\sqrt{3}) = 0.65847\cdots$, thereby partitioning the ordered from the disordered regions in ϵ_2–ϵ_3 space. Specifically, if $K^*(T \to 0; \alpha) > K_c^*$, there exists an onset of long-range order (critical point) at some finite temperature given by $x_c^{(\alpha)}$ where $K^*(x_c^{(\alpha)}) = K_c^*$, with the long-range order parameter increasing as the temperature is lowered, eventually saturating to unity at absolute zero. However, if $K^*(T \to 0; \alpha) < K_c^*$, the region under inspection remains disordered down to absolute zero. Evaluating the parameter $K^*(T \to 0; \alpha)$ requires solely the asymptotic solutions of the cubic algebraic equation (24) for the fugacity.

The search for ground state phase boundaries in the ϵ_2–ϵ_3 space is simplified by the fact that the entire 1st-quadrant (Fig. 2(a)) must be ordered since both interactions are positive, and similarly the entire 3rd quadrant must be disordered since both interactions are negative, so we need to concentrate only on the 2nd and the 4th quadrants. The actual calculations can be simplified even further by using the fluid–magnet correspondence and the symmetry (4) of the magnetic partition function in the J_2–J_3 space. Thus one first obtains the ground state phase boundary in the 2nd quadrant of the ϵ_2–ϵ_3 space by considering the limiting value of $K^*(T \to 0; \alpha)$, using next the fluid–magnet correspondence to obtain the corresponding phase boundary in the J_2–J_3 space for $J_3 > 0$, then using the symmetry in the J_2–J_3 space to obtain the phase boundary for $J_3 < 0$, and finally mapping the latter back to the ϵ_2–ϵ_3 space which gives the phase boundary in the 4th quadrant. The details are found in Appendix B. The resulting ground state phase diagrams are exhibited in Fig. 2.

More particularly, using (28), the $\alpha = 3/2,\ 3$ (red) first-order lines of the fluid in Fig. 2(a) map, respectively, to the $\alpha' = -3,\ 3$ (red) first-order lines of the magnet in Fig. 2(b). Also, the ground-state reduced magnetic field h/J_2 can be conjoined with the ordered state in Fig. 2(b). The conjunction is easily established by substituting the known ground-state values of reduced chemical potential $\mu/|\epsilon_2|$ (see Appendix B) into the phase boundary relation (27) and then transforming α into α' using (28). As notable results, the oblique-lined region in Fig. 2(b) *above* the $J_2 > 0$ axis has ground-state values $h = -(2/3)J_3$, $-3 < \alpha' < 0$ ($h < 0$), and *below* the $J_2 > 0$ axis, $h = -(2/3)J_3$, $0 < \alpha' < 3$ ($h > 0$).

Consequently, one points out that there are thermal phase transitions in the generalized (three-parameter) kagomé Ising model with ferromagnetic pair interactions in the presence of magnetic fields as long as there simultaneously exists an appropriate triplet interaction in competition with the magnetic field. In fact, one notes that the ground-state energies in the oblique-lined region of Fig. 2(b) reveal that their triplet and Zeeman energies exactly cancel one another at absolute zero temperature. Lastly, note that the remarks above are in full compliance with reflection symmetry (4) across the J_2-axis, a symmetry earlier identified in the partition function.

6. Exact phase boundaries and coexistence curves for fixed-point $\alpha = \alpha' = 1$

The case chosen is illustrative, affording a comparatively transparent implementation of the theory. The considered $\alpha = 1$ ray line in ϵ_2–ϵ_3 space (Fig. 2(a)) resides in the 4th quadrant and reveals an ordered ground state. The fluid–magnet correspondence (28) shows that in the corresponding magnet case, this will correspond to $\alpha' = 1$, in the 4th quadrant of the J_2–J_3 plane.

From (26), the value $\alpha = 1$ implies $xy = 1$, which simplifies the solution of the cubic equation (24) enormously, as shown in Appendix B, allowing a simple analytic expression for the physical solution of the fugacity given by (B.16),

$$z = \frac{1}{x^2}[(x-1)^{2/3} - 1]. \tag{34}$$

In the case under study, one proceeds to obtain the resulting companion phase diagrams, viz., phase boundary and co-existence curves.

6.1. The phase boundary

The phase boundary corresponds to the field vs temperature curve in the magnetic case and the chemical potential vs temperature curve in the lattice-gas case. In the present formulation, one starts with the lattice-gas case and obtains the magnetic case using the fluid–magnet correspondence relation (27).

Employing (34) and (10),

$$\begin{aligned} \ln z = \beta\mu &= -2\ln x + \ln[(x-1)^{2/3} - 1] \\ &= -2\beta\epsilon_2 + \ln\left[\left(e^{K_2} - 1\right)^{2/3} - 1\right], \end{aligned} \tag{35}$$

yielding the reduced chemical potential

$$\frac{\mu}{\epsilon_2} = -2 + \frac{1}{K_2}\ln\left[\left(e^{K_2} - 1\right)^{2/3} - 1\right]. \tag{36}$$

In terms of the reduced temperature (29), (36) becomes

$$\frac{\mu}{\epsilon_2} = -2 + \frac{t}{K_{2c}^0}\ln\left[\left(e^{K_{2c}^0/t} - 1\right)^{2/3} - 1\right]. \tag{37}$$

The relation (37) is the sought liquid–vapor phase boundary in reduced variables as displayed in Fig. 3(a). The corresponding magnetic phase boundary is included in Fig. 3(b). Along the above phase boundary (37), the reduced ground state chemical potential is obtained as

$$\lim_{t\to 0}\left(\frac{\mu}{\epsilon_2}\right) = -2 + \frac{2}{3} = -\frac{4}{3}. \tag{38}$$

In order to locate the *critical point*, one needs to calculate its critical coordinates t_c, μ_c/ϵ_2. Towards obtaining t_c, one first substitutes $xy = 1$ and (34) into (21) yielding

$$K^*(\alpha = 1) = \frac{1}{6}\ln[x - 1], \tag{39}$$

where K^* is associated with parameter $\alpha = 1$. At criticality, (39) becomes $K_c^*(\alpha = 1) = \frac{1}{6}\ln[x_c - 1]$, where $K_c^* = \frac{1}{2}\ln[2 + \sqrt{3}] = 0.65847\cdots$ is a critical constant [36] of the traditional honeycomb Ising ferromagnet with purely nearest-neighbor pair interactions. Thus, x_c is found to be

$$x_c(\alpha = 1) = 1 + (2 + \sqrt{3})^3. \tag{40}$$

Finally, using (10), (29) and (40), the reduced *critical temperature* t_c for the current $\alpha = 1$ case becomes

$$\begin{aligned} t_c(\alpha = 1) &= \frac{K_{2c}^0}{K_{2c}(\alpha = 1)} = \frac{K_{2c}^0}{\ln x_c} \\ &= \frac{\ln[3 + 2\sqrt{3}]}{\ln[1 + (2 + \sqrt{3})^3]} = 0.4701\cdots. \end{aligned} \tag{41}$$

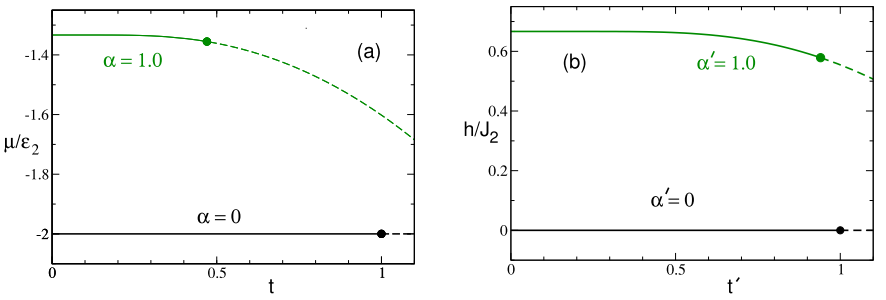

Fig. 3. (a) Liquid–vapor phase boundary where $\alpha \equiv -\epsilon_3/\epsilon_2 = 1$. Plotting (37), the reduced chemical potential μ/ϵ_2 vs reduced temperature t defined in (29). As comparison, the traditional case $\alpha = 0$ is included. The $\alpha = 1$ phase boundary is the monotonically decreasing solid (green) curve beginning at zero temperature with $\mu/\epsilon_2 = -4/3$ and ending at a critical point (solid green circle) whose coordinates are $t_c = 0.4701\cdots$, $\mu/\epsilon_2 = -1.3553\cdots$. The dashed curves are (analytic) extensions of the phase boundary curves into the disordered regions. The dashed green ($\alpha = 1$) curve eventually diverges logarithmically ($\mu/\epsilon_2 \to -\infty$ at $t_{-\infty} = \ln(3+2\sqrt{3})/\ln 2 = 2.69244\cdots$), associated with an empty lattice ($\rho = \rho_{min} = 0$). (b) Corresponding magnetic phase boundary with $\alpha' \equiv -J_3/J_2 = 1$. Plotting (27) with μ/ϵ_2 given by (37), the reduced magnetic field h/J_2 vs reduced temperature t' defined in (30). As a comparison, the traditional case $\alpha' = 0$ is included, satisfying a reduction requirement of the theory. The $\alpha' = 1$ phase boundary is the monotonically decreasing solid (green) curve beginning at zero temperature with $h/J_2 = 2/3$ and ending at a critical point (solid green circle) with coordinates $t'_c (= 2t_c) = 0.9402\cdots$, $h_c/J_2 = 0.5788\cdots$. The dashed green ($\alpha' = 1$) curve eventually diverges logarithmically ($h/J_2 \to -\infty$ at $t'_{-\infty} = 2\ln(3+2\sqrt{3})/\ln 2 = 5.3848\cdots$), associated with a magnetically saturated lattice ($m = m_{min} = -1$).

Directly using (37), the reduced *critical chemical potential* μ_c/ϵ_2 is given by

$$\frac{\mu_c}{\epsilon_2}(\alpha = 1) = -2 + \frac{t_c}{K^0_{2c}} \ln\left[\left(e^{K^0_{2c}/t_c} - 1\right)^{2/3} - 1\right]$$
$$= -2 + \frac{\ln[(2+\sqrt{3})^2 - 1]}{\ln[(2+\sqrt{3})^3 + 1]} = -1.3553\cdots, \tag{42}$$

where (41) and (40) have been used.

In Fig. 3(a), the critical coordinates (41) and (42) locate the critical point (solid circle) which is the end-point of the monotonically decreasing liquid–vapor phase boundary (solid curve).

The corresponding magnetic phase diagram is obtained by using the fluid–magnet relation (27), with μ/ϵ_2 given by (37) and α and t changed to α' and t' using (28) and (31), respectively. The phase boundary curve starts at $t' = 0$ with a value

$$\lim_{t'\to 0}\left(\frac{h}{J_2}\right) = -2 + \frac{8}{3} = \frac{2}{3}. \tag{43}$$

The critical temperature is $t'_c = 2t_c$, using (31) and $\alpha = 1$, where t_c is given by (41). The critical field is given using (27) with critical chemical potential μ_c/ϵ_2 given by (42) and t replaced by $t'/2$. In Fig. 3(b) the critical coordinates t'_c and h_c/J_2 locate the critical point (solid circle) which is the end point of the monotonically decreasing magnetic phase boundary.

As Fig. 3 makes clear, the chemical potential (or field) vs temperature phase boundary is rectilinear in the absence of triplet interactions ($\alpha = \alpha' = 0$); the presence of triplet interactions renders the phase boundary curvilinear. This is an important signature of the addition of triplet interactions. As will be clear later, this has the important consequence that it makes a direct experimental measurement of the magnitude of α' possible.

6.2. The coexistence curve

The coexistence curve corresponds to the magnetization vs temperature curve in the magnetic case and the density vs temperature curve in the lattice-gas case. As before, one obtains the liquid–vapor coexistence curve first and then obtains the magnetic coexistence curve by using the fluid–magnet correspondence relation (33).

In the statistical theory, the *average particle number density* $\rho \equiv \langle N\rangle/\mathcal{N}$ is found in the standard manner from the logarithmic derivative of the grand partition function with respect to a reduced chemical potential, more particularly,

$$\rho = \frac{\langle N\rangle}{\mathcal{N}} = \frac{\partial}{\partial(\beta\mu)}\left[\frac{1}{\mathcal{N}}\ln \Xi(\mu, \mathcal{N}, T)\right]$$
$$= z\frac{\partial}{\partial z}\left[\frac{1}{\mathcal{N}}\ln \Xi(\mu, \mathcal{N}, T)\right] \tag{44}$$

where, as introduced in (10), $z = e^{\beta\mu}$ is the fugacity of the system. In order to calculate the liquid–vapor coexistence curve, $\rho^{coex}_{l,v}$ vs T, it is meaningful to apply a two-stage process. First, one calculates the curvilinear diameter $\rho_{L^*=0}$ vs

T, of the two-phase coexistence region, and then supplements the diameter expression with the required "spontaneous symmetry-breaking" term. Additional useful details of the basic formulation appear in Ref. [29], which examines the inclusion of weak, short-range, repulsive triplet interactions (Axilrod-Teller [15]) using perturbation theory. In contrast, the current theory is closed, considers arbitrary strengths of either competing or cooperating interactions, and the final expressions for phase diagrams are exact and amenable to numerical evaluation using, e.g., Mathematica [37].

Entering (23) into the formula (44) and setting $\mathcal{N}^* = 2\mathcal{N}/3$ yields

$$\rho = \frac{2}{3}z\frac{\partial \ln a^*}{\partial z} - \frac{2}{3}z\frac{\partial \ln(2\cosh L^*)}{\partial z} - z\frac{\partial \ln(\cosh K^*)}{\partial z} + \frac{z}{\mathcal{N}}\frac{\partial \ln Z^*}{\partial L^*}\frac{\partial L^*}{\partial z} + \frac{z}{\mathcal{N}}\frac{\partial \ln Z^*}{\partial K^*}\frac{\partial K^*}{\partial z}. \tag{45}$$

In relation to (45), one obtains from (17) that

$$\frac{\partial \ln Z^*}{\partial L^*} = \mathcal{N}^*\langle\mu\rangle = \frac{2}{3}\mathcal{N}\langle\mu\rangle, \tag{46a}$$

$$\frac{\partial \ln Z^*}{\partial K^*} = \frac{3}{2}\mathcal{N}^*\langle\mu_0\mu_1\rangle = \mathcal{N}\langle\mu_0\mu_1\rangle \tag{46b}$$

whereupon substituting (46) into (45) provides the average particle number density as

$$\rho = \frac{2}{3}z\frac{\partial \ln a^*}{\partial z} - \frac{2}{3}(\tanh L^*)z\frac{\partial L^*}{\partial z} + \frac{2}{3}\langle\mu\rangle z\frac{\partial L^*}{\partial z} + (\langle\mu_0\mu_1\rangle - \tanh K^*)z\frac{\partial K^*}{\partial z}. \tag{47}$$

with $\langle\mu\rangle$ being the honeycomb Ising model magnetization and $\langle\mu_0\mu_1\rangle$ its nearest-neighbor pair correlation.

Towards determining the curvilinear diameter of the liquid–vapor coexistence region, one next evaluates the ρ-expression (47) *at* $L^* = 0$,

$$\rho_{L^*=0} = \frac{2}{3}z\frac{\partial \ln a^*}{\partial z} + (\langle\mu_0\mu_1\rangle - \tanh K^*)z\frac{\partial K^*}{\partial z}, \tag{48}$$

where all quantities in (48) are evaluated at $L^* = 0$, having used the fact that $\langle\mu\rangle_{L^*=0} \equiv 0$ (in *strictly* zero magnetic field, an Ising model with only even-number interactions does not support long-range order, as can be directly proven from symmetry). The nearest-neighbor pair correlation (energy) $\langle\mu_0\mu_1\rangle_{L^*=0}$ is known exactly in terms of complete elliptic integrals [38], and is a continuous monotonically decreasing function of temperature with a weak (energy-type) singularity $\epsilon^*\ln\epsilon^*$ at the critical temperature where $K_c^*/K^* = 1$. The critical constant $K_c^* = \frac{1}{2}\ln(2+\sqrt{3}) = 0.65847\cdots$, and the smallness parameter $\epsilon^* \equiv |(K^* - K_c^*)/K_c^*|$ is, neglecting second order small quantities, the fractional deviation of the temperature from its critical value.

Other than the thermal average $\langle\mu_0\mu_1\rangle_{L^*=0}$, all quantities in (48) can be derived directly once a^* is re-expressed in terms of x, y and z as shown in Appendix C. In (48), as remarked previously, the nearest-neighbor pair correlation $\langle\mu_0\mu_1\rangle_{L^*=0}$ involves complete elliptic integrals (see Houtappel [38]) that can be evaluated exactly by Mathematica. The expressions simplify considerably for the fixed point $\alpha = 1$ ($xy = 1$) and the quantity z (fugacity) is given by (34). Hence, having all needed ingredients in hand for numerical computations, Fig. 4(a) shows, for $\alpha = 1$, the resulting curvilinear diameter $\rho_{L^*=0}$ (dashed curve) exhibiting a negative slope which is more discernible at temperatures closely below the critical temperature.

The liquid and the vapor branches of the coexistence curve, $\rho_{l,v}^{coex}$ vs K_{2c}/K_2, can now be evaluated by adding and subtracting the "spontaneous symmetry breaking" term to expression (48), i.e.,

$$\rho_{l,v}^{coex} = \rho_{L^*=0} \pm \frac{2}{3}\langle\mu\rangle_s\left(z\frac{\partial L^*}{\partial z}\right)_{L^*=0} \tag{49}$$

where the *spontaneous magnetization* $\langle\mu\rangle_s$ (ordering parameter) of the present honeycomb Ising model is foreknown [39] to be

$$\langle\mu\rangle_s = \left(1 - 4\frac{\cosh[3K^*](\cosh[K^*])^3}{(\sinh[2K^*])^6}\right)^{1/8}; \quad 0 \le \frac{K_c^*}{K^*} < 1; \qquad = 0, \quad \frac{K_c^*}{K^*} \ge 1. \tag{50}$$

In the ordered region $0 \le K_c^*/K^* < 1$, the spontaneous magnetization $\langle\mu\rangle_s$ is a continuous monotonically-decreasing function of temperature, and vanishes at the critical temperature where $K_c^*/K^* = 1$ ($K_c^* = 0.65847\cdots$) with a critical exponent 1/8 (algebraic branch point singularity). To evaluate the expression $\left(z\frac{\partial L^*}{\partial z}\right)_{L^*=0}$ in (49), one writes, using (19a),

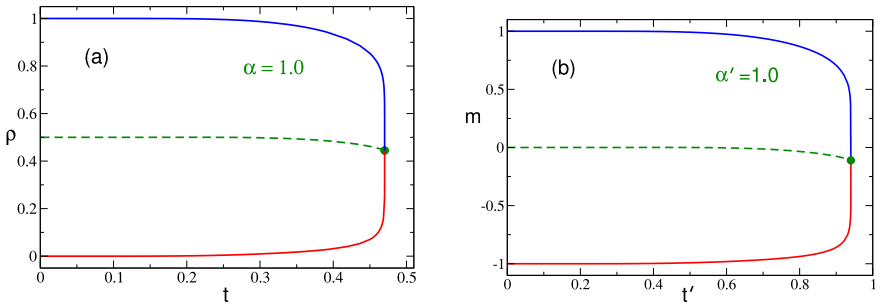

Fig. 4. (a) Liquid–vapor coexistence curve where $\alpha \equiv -\epsilon_3/\epsilon_2 = 1$. Plotting (48) and (49), the particle number density ρ vs (reduced) temperature $t = K_{2c}^0/K_2$, the critical constant $K_{2c}^0 = \ln(3+2\sqrt{3}) = 1.86626\cdots$. The upper (blue) curve is the liquid branch of the coexistence curve and the lower (red) is the vapor branch. The curvilinear diameter of the asymmetric rounded coexistence region is the monotonically decreasing dashed (green) curve which begins at zero temperature with $\rho = 1/2$, and ends at the critical point (solid green circle) whose coordinates are $t_c = 0.4701\cdots$, $\rho_c = 0.4445\cdots$. (b) Corresponding magnetic coexistence curve where $\alpha' \equiv -J_3/J_2 = 1$. Plotting (33) with ρ from (a), the magnetization m vs reduced temperature $t'(= 2t) = K_c^0/K$, $K = \beta J_2$ and the critical constant $K_c^0 = \frac{1}{4}K_{2c}^0 = 0.46656\cdots$. The curvilinear diameter of the asymmetric rounded coexistence region is the monotonically decreasing dashed (green) curve which begins at zero temperature with $m = 0$, and ends at the critical point (solid green circle) whose coordinates are $t_c'(= 2t_c) = 0.9402\cdots$, $m_c = -0.1109\cdots$.

that

$$L^* = \text{arctanh}W = \frac{1}{2}\ln\frac{1+W}{1-W} \tag{51a}$$

where

$$W \equiv \frac{V}{U}\left[\frac{\delta + (C-A)}{\delta - (C-A)}\right]^{1/2}. \tag{51b}$$

Note that $W_{L^*=0} = 0$ since the vanishing of its prefactor V established the zero-field condition $L^* = 0$. As determined and discussed in Ref. [24], the positivity condition $C - A > 0$ is symptomatic with the present positivity (ferromagnetic) condition $K^* > 0$. However, establishing the algebraic sign of $C - A$ via (20a) is more difficult than that for K^* via (21) and (22). The latter only needs the algebraic sign of $l = l(x, y)$ and hence does not require the fugacities z. For the ground state, after obtaining the fugacity in the ordered regions, it can be verified easily (see Appendix B) that the two conditions (namely $C - A > 0$ and $K^* > 0$) are indeed equivalent.

It is laborious but straightforward to obtain the sought result for $\left(z\frac{\partial L^*}{\partial z}\right)_{L^*=0}$ in the coexistence curve expression (49) from (51). The details are left for Appendix C. The final result is (C.10)

$$\left(z\frac{\partial L^*}{\partial z}\right)_{L^*=0} = \frac{(\tanh K^*)^{-1/2}}{U}\left(z\frac{\partial V}{\partial z}\right)_{L^*=0} \tag{52}$$

where $\left(\frac{\partial V}{\partial z}\right)_{L^*=0}$ is given by (C.11), and K^*, U as previously by (21) and (20d), respectively. In the expressions and calculations pertinent to the coexistence curves, x is affiliated with the reduced temperature, $y = x^{-\alpha}$, and z (fugacity) is linked to the reduced chemical potential in the earlier exact phase boundary curves for given values of α. Enlisting Mathematica for the numerical computations, Fig. 4(a) shows, for $\alpha = 1$, the resulting *liquid–vapor coexistence curve* (solid curve) exhibiting an asymmetric rounded shape with a critical point (solid circle). The corresponding magnetic diagram is obtained simply by using (33) and is shown in Fig. 4(b).

7. Results for arbitrary α, α'

The complete solution for arbitrary α requires an exact solution of the general cubic equation (24). While the expressions are not as simple as that in case of $\alpha = 1$, there is no intrinsic difficulty soliciting Mathematica to evaluate the solutions as illustrated in the solution for $\alpha = 1$ in Section 6. The results are qualitatively similar to those for $\alpha = 1$. Fig. 5(a) shows the liquid–vapor phase boundary for two additional values of α, one smaller and one larger than $\alpha = 1$. The results for the corresponding magnetic case for two additional values of α', one smaller and one larger than $\alpha' = 1$, are shown in Fig. 5(b).

Focusing on the magnetic case, Fig. 5(b) shows clearly, for $J_3 < 0$, that as α' increases, (i) the curvature of the field-temperature phase boundary increases, (ii) the critical temperature $t_c'(\alpha')$ decreases, (iii) the critical field $h_c(\alpha')/J_2$ increases, and (iv) the limiting value $h_0(\alpha')/J_2 \equiv \lim_{t'\to 0} h(t';\alpha')/J_2$ increases, all monotonically. This remains true up to $\alpha' = 3$, beyond which the system does not order. These results have an important consequence. For a given fixed α' and a fixed applied magnetic field $h(\alpha')$ in the range $h_c(\alpha') < h(\alpha') < h_0(\alpha')$, sweeping the temperature encounters a discontinuous transition from a "down-spin" ferromagnet to an "up-spin" ferromagnet at a *crossing-point*

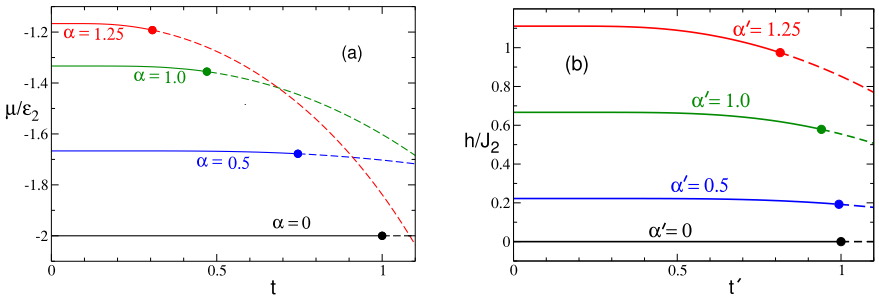

Fig. 5. (a) Changes in the liquid–vapor phase boundary with α, for $\epsilon_3 < 0$. The limiting value $\mu_0/\epsilon_2 \equiv \lim_{t\to 0}\mu(t;\alpha)/\epsilon_2$ increases monotonically from -2 at $\alpha = 0$ to a maximum of -1 at $\alpha = 1.5$, beyond which the system does not order. Similarly the critical points occur at progressively smaller values of t_c and larger values of μ_c/ϵ_2 as α increases. Thus the critical coordinates change from $(t_c = 1, \mu_c/\epsilon_2 = -2)$ for $\alpha = 0$ to $(t_c \to 0, \mu_c/\epsilon_2 \to -1)$ in the limit of $\alpha \to 1.5$. (b) Changes in the corresponding magnetic phase boundary with α', for $J_3 < 0$. The limiting value $h_0/J_2 \equiv \lim_{t'\to 0} h(t';\alpha')/J_2$ increases monotonically from 0 at $\alpha' = 0$ to a maximum of 2 at $\alpha' = 3$, beyond which the system does not order. Similarly the critical points occur at progressively smaller values of t_c and larger values of h_c/J_2 as α' increases. Thus the critical coordinates change from $(t_c' = 1, h_c/J_2 = 0)$ for $\alpha' = 0$ to $(t_c' \to 0, h_c/J_2 \to 2)$ in the limit of $\alpha' \to 3$.

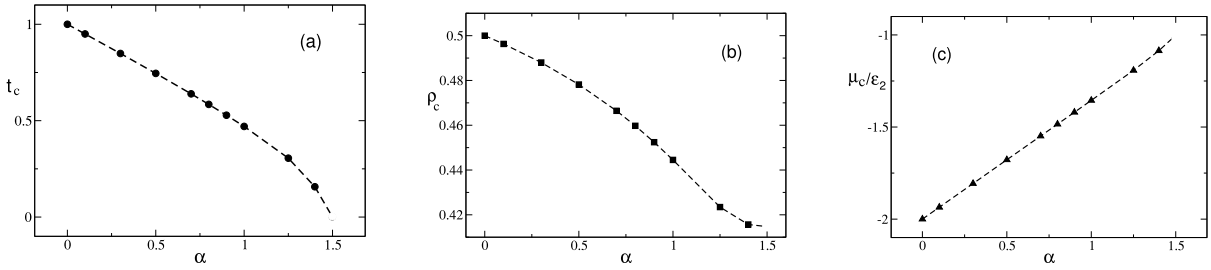

Fig. 6. Prominent critical constants vs α for the generalized lattice gas model. The solid symbols are exact calculated values, the dashed line is a guide to the eye. The figure pertains to the 4th quadrant of ϵ_2–ϵ_3 space. The critical constants are each plotted for the range of values $0 \le \alpha < 3/2$, where $\alpha \equiv -\epsilon_3/\epsilon_2$. (a) Reduced critical temperature t_c vs α. (b) Critical density ρ_c vs α. (c) Reduced critical chemical potential μ_c/ϵ_2 vs α.

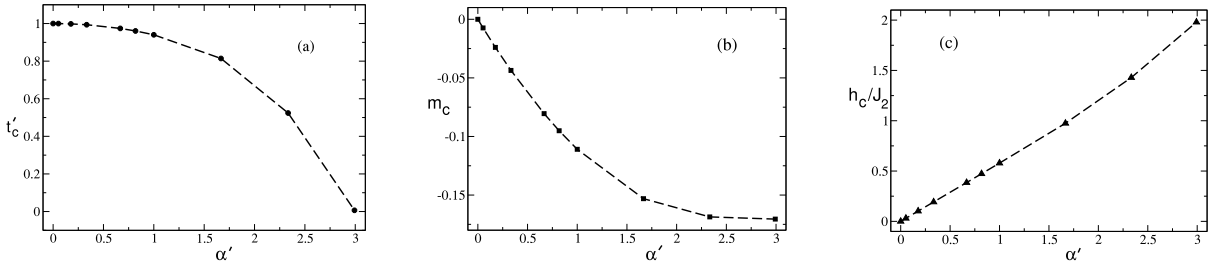

Fig. 7. Prominent critical constants vs α' for the generalized Ising magnet. The solid symbols are exact calculated values, the dashed line is a guide to the eye. The figure pertains to the 4th quadrant of J_2–J_3 space. The critical constants are each plotted for the range of values $0 \le \alpha' < 3$, where $\alpha' \equiv -J_3/J_2$. (a) Reduced critical temperature t_c' vs α'. (b) Critical magnetization m_c vs α'. (c) Reduced critical field h_c/J_2 vs α'.

temperature $t'_{crossing}(\alpha')$. By locating the crossing-point temperature for different values of the magnetic field, one can therefore experimentally determine the entire field-temperature phase boundary. This amounts to a direct and precise measurement of the parameter α', and therefore of the magnitude of the triplet interaction if the pair interaction is known from other measurements. The symmetry (4) of the partition function allows one to obtain results for $J_3 > 0$.

Figs. 6 and 7 show select critical constants as functions of α and α', respectively.

8. Discussion and summary

Exact results in physics are valuable for a variety of reasons. Endeavoring to retain and emphasize only the most essential elements of a physical problem (akin to cartoonists), exact solutions of simple model systems often provide definite guidance and insights on more realistic and invariably more mathematically complex systems. Exact results in tractable models of seemingly different physical systems may alert researchers to significant common features of the systems and actually accentuate concepts of universality. In addition to their own aesthetic appeal, exact results can,

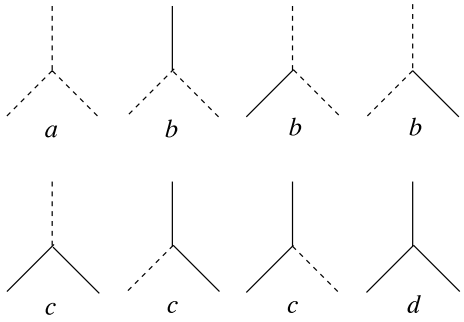

Fig. A.8. Vertex configurations and associated weights for the symmetric eight-vertex model. Solid (dashed) edges denote the edges as bond occupied (empty).

of course, serve as standards against which both approximation methods and approximate results may be appraised. Also, the underlying mathematical structures of integrable lattice models are rich in content and have led to important developments in mathematics.

Theoretical studies of strongly correlated systems in condensed matter physics primarily consider two-particle interactions. However, particularly at higher densities, multi-particle interactions can be germane and lead to significant effects [40]. Taking advantage of a generalized fluid–magnet correspondence, the present paper theoretically investigated the finite-field induced phase transitions of a kagomé Ising ferromagnet, and the condensation of a kagomé lattice gas, both with pair and triplet interactions. Exact ground-state phase diagrams as well as all possible phase boundary curves (chemical potential and field vs temperature) and companion coexistence curves (density and magnetization vs temperature) of both the fluid and magnet were determined. For a special case of competing interactions, an illustrative implementation of the theory was developed. In particular, the field-temperature phase boundary changes from a rectilinear form at zero triplet interaction to a curvilinear form at finite triplet interaction. The curvilinear shape enhances prospects of experimentally detecting field-induced discontinuous transitions from a "down-spin" ferromagnet to an "up-spin" ferromagnet for ranges of magnetic fields and temperatures. The latter ranges are dependent upon the relative magnitude of the triplet and pair interaction parameters, as illustrated in Fig. 5(b). Prominent critical constants of the fluid and the magnet are plotted as functions of the ratio of interaction parameters.

Considering Fig. 5, one recognizes that exploring the phase boundary systematically provides a handle to identify the existence and importance of triplet interactions in general. With sensitive enough experiments, one should be able to observe the effects of even a very small triplet interaction in the presence of a more dominant pair interaction, which situation is expected to be quite ubiquitous in nature.

This paper is devoted to only the ferromagnetic (ordered) region. For antiferromagnetic pair-interactions, there is no long range order. However, it has been shown [41] that disordered regions can be very different (with or without frustration) if either pair or triplet interactions dominate. Studies of the generalized kagomé Ising model in these disordered regions are ongoing.

Acknowledgment

The authors wish to express their gratitude to F.Y. Wu for his valuable correspondences and unique insights on the present investigations.

Appendix A. Honeycomb eight-vertex model and proof of Eq. (14)

Consider a honeycomb lattice (Fig. 1, dashed edges) and draw bonds along its edges such that each edge is independently "traced" (occupied) or left "open" (empty). Then, there are eight different vertex configurations occurring at a vertex which are shown in Fig. A.8. With each configuration, one associates a vertex weight a, b, c, d, and the weights are assumed to be positive. In Fig. A.8, note that the assignment of weights does not distinguish bonds in different directions, thereby specializing our attention to a *symmetric* eight-vertex model.

The partition function of the eight-vertex model [23,24,26,27,34] is the graph generating function

$$Z_{8V}(a,b,c,d) = \sum a^{n_0} b^{n_1} c^{n_2} d^{n_3} \tag{A.1}$$

where the summation is taken over all bond configurations of the lattice, and n_i is the number of vertices having i bonds. As seen shortly, in the statistical theory of phase transitions and criticality, the vertex weights reveal themselves as

Boltzmann factors

$$a = \exp[-\beta\tilde{\epsilon_0}], \quad b = \exp[-\beta\tilde{\epsilon_1}],$$
$$c = \exp[-\beta\tilde{\epsilon_2}], \quad d = \exp[-\beta\tilde{\epsilon_3}], \tag{A.2}$$

where $\tilde{\epsilon_i}$ is the pertinent energy of a vertex having i bonds. Here $\beta \equiv 1/k_BT$, where k_B is the Boltzmann constant and T the absolute temperature.

The grand canonical partition function (8) of the generalized kagomé lattice gas model (5) can be written in terms of the Boltzmann factor of a triangular face

$$\Omega(n_i, n_j, n_k) = e^{\frac{\beta\mu}{2}(n_i+n_j+n_k)+K_2(n_in_j+n_in_k+n_jn_k)+K_3n_in_jn_k} \tag{A.3}$$

as

$$\Xi(\mu, \mathcal{N}, T) = \sum_n \prod_{\langle i,j,k\rangle} \Omega(n_i, n_j, n_k), \tag{A.4}$$

where the summation symbol n represents the set of total $\mathcal{N}$ lattice gas variables and, imposing periodic boundary conditions, the product is taken over the total $2\mathcal{N}/3$ elementary triangles.

In Fig. 1, one observes that the midpoints of the edges of the associated honeycomb lattice may be viewed as the sites of the kagomé lattice. In this setting, every occupation number variable resides on one edge of the honeycomb lattice. If one regards the lattice-gas variable $n = 0$ as implying that the edge on which n resides is covered by a bond, and $n = 1$ as implying that the edge is empty, then the partition function (A.4) describes precisely the eight-vertex model partition function (A.1) with the vertex weights, using (A.3),

$$a = \Omega(1, 1, 1) = x^3yz^{3/2}, \tag{A.5a}$$
$$b = \Omega(1, 1, 0) = xz, \tag{A.5b}$$
$$c = \Omega(1, 0, 0) = z^{1/2}, \tag{A.5c}$$
$$d = \Omega(0, 0, 0) = 1, \tag{A.5d}$$

where x, y and z are given by (10). Succinctly, one has established the *partition function equivalence* (14)

$$\Xi(\mu, \mathcal{N}, T) = Z_{8V}(a, b, c, d), \tag{A.6}$$

where the vertex weights a, b, c, d are given by (A.5), and $Z_{8V}(a, b, c, d)$, $\Xi(\mu, \mathcal{N}, T)$ by (A.1), (A.4), respectively.

In the preceding arguments, one is perfectly free to oppositely choose the lattice-gas variable $n = 1$ as implying that the edge on which n resides is covered by a bond, and $n = 0$ as implying that the edge is empty. In other words, one simply interchanges the "traced" and "open" edges in Fig. A.8. Then, one arrives at the result that the RHS of (A.6) becomes $Z_{8V}(d, c, b, a)$, illustrating a known reflection symmetry [23] $Z_{8V}(a, b, c, d) = Z_{8V}(d, c, b, a)$ of the eight-vertex model.

Appendix B. Ground state phase diagram from $T \to 0$ limit of K^*

In order to obtain the ground state phase diagram, one first needs to evaluate the parameter $K^*(T \to 0)$. This will require the asymptotic solutions of the cubic equation for the fugacity z (24). In this Appendix, the solutions of the cubic equation will be written down first and the $T \to 0$ limits for various regions in the ϵ_2–ϵ_3 as well as J_2–J_3 spaces will be obtained using the solutions of the cubic equation.

B.1. Solution of the cubic equation

The cubic equation in (24) can be solved exactly for its real (physical) solution. Define

$$Q \equiv \frac{1}{9}(3a_1 - a_2^2); \quad R \equiv \frac{1}{54}(9a_1a_2 - 27a_0 - 2a_2^3), \tag{B.1a}$$

and the discriminant is

$$D = Q^3 + R^2. \tag{B.1b}$$

If the discriminant is positive, then there is one real solution for z, the other two being complex conjugates of one another. The real fugacity solution is given by

$$z \equiv z_1 = S_1 + S_2 - \frac{1}{3}a_2, \quad S_1 \equiv (R + \sqrt{D})^{1/3},$$
$$S_2 \equiv (R - \sqrt{D})^{1/3}. \tag{B.2}$$

In the current calculations, it is also useful to write Q, R, D as explicit functions of x, y. Substituting (24) into (B.1) yields

$$Q = -\frac{(-1+xy+x^2y-x^3y^2)^2}{x^6y^2(2-3xy+x^3y^2)^2}, \tag{B.3a}$$

$$D = \frac{(-1+x^2y)^6}{4x^{16}y^4(2-3xy+x^3y^2)^4} \times D_1,$$

$$D_1 = -3-6x^2y+x^4y^2+4x(1+y), \tag{B.3b}$$

$$R = \frac{(-1+x^2y)^3}{2x^9y^3(2-3xy+x^3y^2)^3} \times R_1$$

$$R_1 = 2-6xy+3x^2y^2-6x^4y^3+x^6y^4 + 2x^3y^2(2+y). \tag{B.3c}$$

The fractional algebraic forms (B.3) were obtained using symbolic computation by Mathematica [37].

In the present context of phase transitions and criticality, theoretical investigations upon the (close-packed) kagomé lattice need only consider dominant attractive (ferromagnetic) cases $K^* > 0$ (21). As commented in Section 3, l defined in (22) is positive in all such cases. Note that D_1 of (B.3b) equals l, implying that the discriminant $D > 0$. Concisely, K^*, l, D have positive algebraic sign in all cases of interest.

It develops that there are regimes where there is no positive solution for the fugacity z so that the solutions are unphysical. These regimes can be identified directly from the zero temperature limits of the coefficient a_0 (24d). We note that the product of the three roots of the cubic equation satisfies the condition

$$z_1z_2z_3 = -a_0. \tag{B.4}$$

When the discriminant D (B.1b) is positive, which is the case whenever $K^* > 0$, there is only one real root and the other two are complex conjugates of one another. For z_2 and z_3 complex conjugate of each other, $z_2z_3 > 0$. Thus the real solution $z = z_1$ has the opposite sign of a_0. In other words, a real positive solution for the fugacity requires $a_0 < 0$. We will exploit this result to identify regions where there is no physical solution for fugacity, indicating that there is no phase transition.

B.2. $T \to 0$ limit of K^*

By investigating the zero temperature limits of K^* (21) and comparing them with K_c^* one can separate the disordered states from the ordered states. If $K^*(T \to 0; \alpha) > K_c^*$, there exists a phase transition at some finite temperature given by x_c where $K^*(x_c; \alpha) = K_c^*$, while if $K^*(T \to 0; \alpha) < K_c^*$ the state remains disordered down to zero temperature. Evaluating the parameter $K^*(T \to 0)$ will require only the asymptotic solutions of the cubic equation for the fugacity z (24).

As alluded to in Section 5, it is sufficient to consider the second quadrant of the ϵ_2–ϵ_3 plane of Fig. 2(a), where $\epsilon_2 < 0$ and $\epsilon_3 > 0$, to check the existence of the liquid–vapor phase boundary. The first quadrant has only positive (attractive) interactions, leading to ordered states, while the third quadrant has only negative (repulsive) interactions, leading to disordered states. The fourth quadrant does have competing interactions and does have a phase boundary, but this will be obtained directly by appealing to the symmetry in the corresponding J_2–J_3 plane.

B.2.1. 2nd quadrant in Fig. 2 ($\epsilon_2 < 0$, $\epsilon_3 > 0$, $\alpha > 0$)

For $\epsilon_2 < 0$, we have $x < 1$. For $\alpha > 0$, we have $y = x^{-\alpha} > 1$. Now the asymptotic analysis for $t \to 0$ requires $x \to 0$. As we will see, in this regime, considerations of K^* vs K_c^* will tell us that ordered states occur only for $\alpha > 3$.

Case I: $\alpha > 3$:

In this regime, we have from (B.3b), (B.3c) and (24b)

$$D \to \frac{1}{4}\frac{1}{x^{12-4\alpha}}; \quad R \to \frac{1}{2}\frac{1}{x^{6-2\alpha}}; \quad a_2 \to -\frac{6}{x^{5-2\alpha}} \tag{B.5}$$

which gives, using (B.2),

$$z(x \to 0) \to x^{2(\alpha-3)/3}; \quad \alpha > 3. \tag{B.6}$$

Again as before, from (21),

$$K^* \to \frac{1}{4}\ln[1+\frac{1}{x^{2(\alpha-3)/3}}]; \quad \alpha > 3. \tag{B.7}$$

Since the exponent of $x < 1$ inside the logarithm increases for $\alpha > 3$ leading to $K^*(x) = K_c^*$ for some $x = x_c$, there will be a phase transition and the zero temperature state will be an ordered state. As we will see below, there is no phase transition for $\alpha \leq 3$.

The ground state chemical potential can be obtained from (B.6). Since $\epsilon_2 < 0$, one needs to be careful about the sign of $\frac{\mu}{\epsilon_2}$:

$$\frac{\mu}{|\epsilon_2|}(t \to 0; \alpha) = -\frac{2}{3}(\alpha - 3); \quad \alpha > 3. \tag{B.8}$$

The quantity $C - A$ in (19) plays an important role in the Wu theory [24]. One can compute this quantity from (20a), this time in the limit $x \to 0$. Rewriting

$$C - A = z[(xy - 1)x^2z - 1 + x] \to z[(x^3yz - 1)] \tag{B.9}$$

and using (B.6) one obtains, for $\alpha > 3$,

$$\frac{C - A}{z} \to x^{3-\alpha}x^{2(\alpha-3)/3} - 1 \to x^{1-\alpha/3} - 1, \tag{B.10}$$

which is positive since $x \to 0$ and $\alpha > 3$. This confirms the result [24] that $C - A > 0$ when $K^* > 0$.

Case II: $\alpha = 3$:
In this case $x^3y = 1$, $x < 1$, $y > 1$. In the limit $x \to 0$, from (B.3b), (B.3c) and (24b) we obtain

$$D \to 1; \quad R \to \frac{3}{2}; \quad a_2 \to -6x. \tag{B.11}$$

This gives, utilizing (B.2), $z_1 \to c$ where $c = (5/2)^{1/3} + (1/2)^{1/3} \approx 2.15091$. Corresponding K^* is given by (21),

$$K^* \to \frac{1}{4}\ln\left[1 + \frac{5c}{(c-1)^2}\right] \to 0.552594 < K_c^*. \tag{B.12}$$

Thus there is no phase transition for $\alpha = 3$. Similar argument shows that there is no phase transition for $\alpha < 3$. The line $\alpha = 3$ separates ordered and disordered regions.

Using the fluid–magnet correspondence relation between α and α' given in (28), one immediately sees that in the corresponding J_2–J_3 space the phase boundary line is given by $\alpha' = -3$, shown in Fig. 2(b).

B.2.2. 4th quadrant in Fig. 2 ($\epsilon_2 > 0$, $\epsilon_3 < 0$, $\alpha > 0$)

The symmetry (4) of the magnetic partition function implies that if there is a phase boundary for $\alpha' = -3$ in the J_2–J_3 space as shown above, there must be a phase boundary for $\alpha' = +3$, as shown in Fig. 2(b). Using the reverse mapping of (28), this immediately implies that there is a phase boundary at $\alpha = 3/2$ in the ϵ_2–ϵ_3 space, as shown in Fig. 2(a).

This completes the ground state phase diagrams in both ϵ_2–ϵ_3 and J_2–J_3 spaces, completing Fig. 2(a) and (b).

B.3. Special Case $\alpha = 1$

For the special case $\alpha = 1$ considered in Section 6 one has, from (26),

$$xy = 1. \tag{B.13}$$

Then, using (B.13), expressions (B.3) easily simplify as

$$Q = 0, \quad R = \frac{(x-1)^2}{2x^6}, \quad D = R^2 > 0. \tag{B.14}$$

Using (B.13) and (B.14), expressions (B.2) and (24) similarly simplify as

$$S_1 = (2R)^{1/3} = \frac{(x-1)^{2/3}}{x^2}, \quad S_2 = 0, \quad a_2 = \frac{3}{x^2}, \tag{B.15}$$

jointly yielding the (physical) fugacity

$$\begin{aligned} z = z_1 &= S_1 + S_2 - \frac{1}{3}a_2 \\ &= \frac{1}{x^2}[(x-1)^{2/3} - 1]. \end{aligned} \tag{B.16}$$

Appendix C. Coexistence curve

In (47), several partial derivatives are needed to evaluate the density at $L^* = 0$. First, a^* can be expressed in terms of x, y and z as [29]

$$a^* = \frac{qr}{(2s)^{3/2}} \tag{C.1}$$

where

$$q \equiv 1 - 2fz^{-1/2}\eta, \tag{C.2a}$$
$$r \equiv (1+xz)\eta + (1+x^3yz)z^{1/2}, \tag{C.2b}$$
$$s \equiv 1 - \nu\eta, \tag{C.2c}$$

with

$$\eta = -\nu + (1+\nu^2)^{1/2}, \tag{C.2d}$$
$$\nu = fz^{-1/2} + gz^{1/2}, \tag{C.2e}$$
$$f \equiv f(x,y) = \frac{1-x}{(x^2y-1)x}, \tag{C.2f}$$
$$g \equiv g(x,y) = \frac{(xy-1)x}{x^2y-1}. \tag{C.2g}$$

Using (C.1), (48) becomes

$$\rho_{L^*=0} = \frac{2}{3}\left(z\frac{\partial \ln q}{\partial z} + z\frac{\partial \ln r}{\partial z}\right) - \frac{\partial \ln s}{\partial z} + (\langle \mu_0\mu_1\rangle - \tanh K^*)z\frac{\partial K^*}{\partial z}. \tag{C.3}$$

where all quantities in (C.3) are evaluated at $L^* = 0$, The individual terms are given by

$$z\frac{\partial \ln q}{\partial z} = \frac{z}{q}\frac{\partial q}{\partial z} = -\frac{f\{[(\nu(1+\nu^2)^{-1/2}-1)(g-fz^{-1}) - z^{-1/2}]\}}{1-2fz^{-1/2}[(1+\nu^2)^{1/2}-\nu]},$$
$$z\frac{\partial \ln r}{\partial z} = \frac{z}{r}\frac{\partial r}{\partial z} = \frac{c_1+c_2}{c_0};$$
$$c_1 = \frac{1}{2}(1+xz)[\nu(1+\nu^2)^{-1/2}-1](gz^{1/2} - fz^{-1/2});$$
$$c_2 = xz[(1+\nu^2)^{1/2}-\nu] + \frac{1}{2}z^{1/2}(1+3x^3yz);$$
$$c_0 = (1+xz)[(1+\nu^2)^{1/2}-\nu] + z^{1/2}(1+x^3yz);$$
$$z\frac{\partial \ln s}{\partial z} = \frac{z}{s}\frac{\partial s}{\partial z} = \frac{(fz^{-1/2} - gz^{1/2})[(1+2\nu^2)(1+\nu^2)^{-1/2} - 2\nu]}{2\{1-\nu[(1+\nu^2)^{1/2}-\nu]\}}, \tag{C.4}$$

and

$$z\frac{\partial K^*}{\partial z} = \frac{z[x-1-x^2(xy-1)z]}{4[x-1+x^2(xy-1)z]} \times \frac{l}{[x-1+x^2(xy-1)z]^2 + lz} \tag{C.5}$$

where l [Eq. (22)], f, g are each functions solely of x, y.

Eq. (51b) can be written as

$$W = \frac{V}{U}\left[\frac{\frac{\delta}{C-A}+1}{\frac{\delta}{C-A}-1}\right]^{1/2} = \frac{V}{U}\left[\frac{e^{2K^*}+1}{e^{2K^*}-1}\right]^{1/2} = V\cdot\frac{(\tanh K^*)^{-1/2}}{U} \tag{C.6}$$

Then, (51a) yields

$$2\frac{\partial L^*}{\partial z} = \frac{[(1-W)\frac{\partial W}{\partial z} - (1+W)(-\frac{\partial W}{\partial z})]/(1-W)^2}{(1+W)/(1-W)} = 2\frac{\partial W}{\partial z}/(1-W^2) \tag{C.7}$$

implying that

$$\left(\frac{\partial L^*}{\partial z}\right)_{L^*=0} = \left(\frac{\partial W}{\partial z}\right)_{L^*=0}, \tag{C.8}$$

having substituted the fact that $W_{L^*=0} = 0$. Differentiating (C.6) via the product rule, one obtains the RHS of (C.8) as

$$\left(\frac{\partial W}{\partial z}\right)_{L^*=0} = \frac{(\tanh K^*)^{-1/2}}{U}\left(\frac{\partial V}{\partial z}\right)_{L^*=0}, \tag{C.9}$$

again utilizing the mutual null condition $V = 0$ at $L^* = 0$. Hence, cascading perusal of (C.8) and (C.9) directly provides the sought result for $\left(z\frac{\partial L^*}{\partial z}\right)_{L^*=0}$ in the coexistence curve expression (49), viz.,

$$\left(z\frac{\partial L^*}{\partial z}\right)_{L^*=0} = \frac{(\tanh K^*)^{-1/2}}{U}\left(z\frac{\partial V}{\partial z}\right)_{L^*=0} \tag{C.10}$$

Note that from (C.2b) and (20d), $U = r$. Also employing the V-expression (20e), its derivative at $L^* = 0$ is calculated to be

$$\begin{aligned}\left(\frac{\partial V}{\partial z}\right)_{L^*=0} &= \frac{1}{2}[\nu(1+\nu^2)^{-1/2} - 1] \\ &\times (z^{-1/2} + x^3yz^{1/2})(gz^{1/2} - fz^{-1/2}) - x \\ &+ \frac{1}{2}[(1+\nu^2)^{1/2} - \nu](z^{-1/2} + 3x^3yz^{1/2}).\end{aligned} \tag{C.11}$$

References

[1] S.G. Brush, Rev. Modern Phys. 39 (1967) 883;
M.E. Fisher, in: W.E. Brittin (Ed.), Lectures in Theoretical Physics, Vol. VIIC, Univ. of Colorado Press, Boulder, Colorado, 1965, p. 1.
[2] R.J. Baxter, Exactly Solved Models in Statitical Mechanics, Academic, New York, 1982.
[3] J.M. Thijssen, Computational Physics, second ed., Cambridge, 2007.
[4] W. Krauth, Statistical Mechanics: Algorithms and Computations, Oxford, 2006.
[5] K. Binder, D. Heermann, Monte Carlo Simulation in Statistical Physics: An Introduction, fifth ed., Springer, 2010.
[6] S. Ranjbar, Chinese, J. Phys. 41 (2003) 383.
[7] E. Ibarra-Garcia-Padilla, F.J. Poveda-Cuevas, C.G. Malanche-Flores, cond-mat arXiv:1606.05800v2, 2016.
[8] S. Froyen, A.A.S. Sudbo, P.C. Hemmer, Physica A 85 (1976) 399.
[9] Z.-Y. Wang, S.C. Furuya, M. Nakamura, R. Komakura, Phys. Rev. B 88 (2013) 224419.
[10] R.J. Baxter, F.Y. Wu, Phys. Rev. Lett. 31 (1973) 1294.
[11] F.C. Alcaraz, J.L. Cardy, S. Ostlund, J. Phys. A: Math. Gen 16 (1983) 159.
[12] A. Hintermann, D. Merlini, Phys. Lett. A 41 (1972) 208.
[13] Y. Huang, Y. Deng, J.L. Jacobsen, J. Salas, Nuclear Phys. B 868 [FS] (2013) 492.
[14] J. Strečka, Entropy 20 (2018) 91.
[15] B.M. Axilrod, E. Teller, J. Chem. Phys. 11 (1943) 299.
[16] M.W. Pestak, R.E. Goldstein, M.H.W. Chan, J.R. de Bruyn, D.A. Balzarini, N.W. Ashcroft, Phys. Rev. B 36 (1987) 599.
[17] N.S. Sullivan, Bull. Magn. Reson. 11 (1989) 86, See http://www.weizmann.ac.il/ISMAR/bulletin/volume-11 and references cited therein;
J.M. Delrieu, N.S. Sullivan, Phys. Rev. B 23 (1981) 3197.
[18] M. Roger, J.J. Hetherington, J.M. Delrieu, Rev. Modern Phys. 55 (1983) 1.
[19] J.K. Pachos, M.B. Plenio, Phys. Rev. Lett. 93 (2004) 056402.
[20] C. D'Cruz, J.K. Pachos, Phys. Rev. A 72 (2005) 043608.
[21] I. Bloch, J. Dalibard, W. Zwerger, Rev. Modern Phys. 80 (2008) 885.
[22] R.J. Baxter, Physica A 106 (1981) 18.
[23] F.Y. Wu, J. Math. Phys. 15 (1974) 687.
[24] X.N. Wu, F.Y. Wu, J. Stat. Phys. 50 (1988) 41.
[25] K.Y. Lin, B.H. Chen, Internat. J. Modern Phys. B4 (1990) 123.
[26] X.N. Wu, F.Y. Wu, J. Phys. A: Math. Gen. 22 (L55) (1989) L1031.
[27] F.Y. Wu, X.N. Wu, Phys. Rev. Lett. 63 (1989) 465.
[28] Later, the same result was obtained by Wu [34] using a direct mapping without using a weak-graph transformation.
[29] J.H. Barry, N.S. Sullivan, Internat. J. Modern Phys. B7 (1993) 2831.
[30] M.E. Fisher, Proc. Roy. Soc. A 254 (1960) 66; Proc. Roy. Soc. A 256 (1960) 502.
[31] L.L. Liu, H.E. Stanley, Phys. Rev. B 10 (1974) 2958.
[32] The Ising spin magnetic moment $m(\equiv g\mu_B/2$ in standard spectroscopic notation) actually appears in the Zeeman energy as $-mh\sum_i \sigma_i$, but is omitted for notational simplicity. When needed, m can be reentered at the conclusion of the calculation.
[33] As stated, the two-dimensional kagomé lattice (Japanese woven bamboo pattern) is a semiregular (archimedean) lattice. In two-dimensions, the only regular (platonic) lattices are the honeycomb, square and triangular.
[34] F.Y. Wu, J. Phys. A: Math. Gen. 23 (1990) 375.
[35] See, for example, R.B. Griffiths, in: C. Domb, M.S. Green (Eds.), Phase Transitions and Critical Phenomena, Vol. 1, Academic, New York, 1972.
[36] See, for example, I. Syozi, in: C. Domb, M.S. Green (Eds.), Phase Transitions and Critical Phenomena, Vol. 1, Academic, New York, 1972.
[37] S. Wolfram, The Mathematica Book, fifth ed., Wolfram Media, 2003.
[38] R.M.F. Houtappel, Physica 16 (1960) 425.
[39] S. Naya, Progr. Theoret. Phys. 11 (1954) 53, I. Syozi, Ref. [36];
J.H. Barry, T. Tanaka, M. Khatun, C.H. Múnera, Phys. Rev. B 44 (1991) 2595, and references cited therein.
[40] See,for example, J.H. Barry, K.A. Muttalib, T. Tanaka, J. Phys. A 45 (2012) 494019, and references cited therein.
[41] K.A. Muttalib, M. Khatun, J.H. Barry, Phys. Rev. B 96 (2017) 184411.